Computational models for fusion of texture and color: a comparative study

Hui-Liang Shen
John H. Xin
The Hong Kong Polytechnic University
Institute of Textiles and Clothing
Hung Hom, Kowloon
Hong Kong, China
E-mail: tcshenhl@polyu.edu.hk; tcxinjh@inet.polyu.edu.hk

Abstract. *Fusion of texture and color is to simulate color texture images that are perceptually very close to the actual ones. There are three computational models, i.e., gray-to-color mapping (GCM), color-to-color mapping (CCM), and dichromatic-based (DICH) models. The CCM model is extended to three methods, namely, CCM-RGB, CCM-LCH, and CCM-l$\alpha\beta$, when it is applied in different color spaces. The DICH model contains two methods: DICH-GC and DICH-CC, considering the original image can be either gray scale or color. The color fidelity of these six methods is comparatively investigated in terms of image similarity between simulated and target images.* © *2005 SPIE and IS&T.* [DOI: 10.1117/1.1990007]

1 Introduction

Texture and color are two important properties of images. The description of texture and color has been widely studied in the domain of image segmentation and texture synthesis.[1,2] Texture image segmentation considers the separation of a different object area by analyzing the statistical distribution of texture and color,[1] while texture synthesis deals with the generation of new representative texture samples from the underlying stochastic process of original ones.[2] In the literature of image processing, the pseudocoloring technique is always used to render gray-scale images for visualization.[3] However, color fidelity is usually not the objective of the texture synthesis and pseudocoloring techniques.

This paper studies the fusion of texture and color for the simulation of new texture images with special consideration of color fidelity. More precisely, given an original image and a solid target color, the objective is to simulate a new color texture image that is a close replica of the target image so that the final style of the textured object can be visualized before it is actually produced. For example, in the textile and apparel industry, as the final products such as colored fabrics are textured, there are demands for the mapping of solid colors to various texture patterns for visualization and for color quality control.

Currently, several computational models have been reported for the fusion of texture and color information. Xin and Shen investigated the interchannel relationship among the spatial distribution of the red, green, and blue (RGB) channels of texture images, and then proposed a method for the color mapping of texture images.[4] The numerical and psychophysical experiment results indicated that the model performs well in terms of color difference. Combined with image segmentation, the color mapping method could be applied in the recoloring of textile printing designs.[5] Botchko *et al.* analyzed the relationship between the mean spectral reflectance and the standard deviation of natural objects and proposed parametric methods for the virtual recoloring of texture images.[6,7] Based on the dichromatic reflection model introduced by Shafer,[8] Shen and Xin further developed a method for the rendering of texture images with high color accuracy.[9] Reinhard *et al.* proposed a color transfer method using a recently developed $l\alpha\beta$ color space,[10] and the method works well in changing the color distribution of natural scene images. Montag and Berns presented a method to simulate textile color texture images in the CIELCH color space using singular value decomposition (SVD) technique.[11] It is noted that the methods proposed in Refs. 4–7, 10, and 11 are all based on the statistical analysis of the texture and color distribution in texture images, while the texture rendering method in Ref. 9 is based on the physical interaction between texture surfaces and incident light.

In this paper, we first investigate the channel correlation among different channels of texture images and discuss the interaction based on the dichromatic reflection model.[8] Different computational models for texture and color fusion are then presented. Finally, the color accuracy of these models is comparatively investigated in terms of image similarity.

2 Statistical Analysis and Physical Model for Texture Images

The texture images used in this paper were collected by imaging textile fabrics. The textile fabrics were dyed using different colored dyestuffs, and the different texture patterns are due to different woven methods, such as plain and twill woven. In this paper, the textile fabrics used were all single colored; multicolored fabrics were not considered.

For a typical three-channel RGB imaging device such as a digital camera or a scanner, the response u_n^p of channel n at pixel p is given as

Paper 04143R received Aug. 19, 2004; revised manuscript received Feb. 21, 2005; accepted for publication Feb. 23, 2005; published online Jul. 19, 2005.
1017-9909/2005/14(3)/033003/7/$22.00 © 2005 SPIE and IS&T.

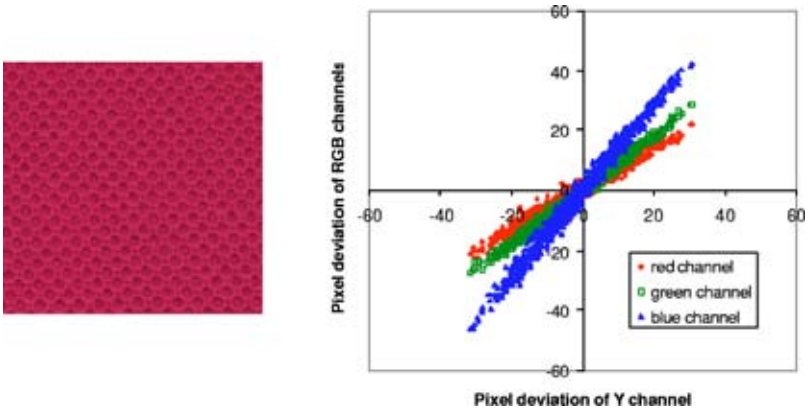

Fig. 1 Color texture image (left) and the pixel deviation relationship between red, green, and blue channels and *Y* channel (right). The correlation coefficients of red, green, and blue channels with respect to *Y* channel are 0.985, 0.915, and 0.988, respectively.

$$u_n^p = \int l(\lambda) r(\lambda, p) s_n(\lambda)\, d\lambda \quad n = 1, 2, 3 \text{ or RGB}, \tag{1}$$

where λ denotes wavelength, $l(\lambda)$ is the spectral power distribution of the illumination, $s_n(\lambda)$ is the spectral sensitivity function of the n'th sensor, and $r(\lambda, p)$ is the spectral reflectance of object at position p. Note that Eq. (1) supposes that the outputs of the imaging device are linear with the flux of incoming light intensity. The luminance u_Y^P at pixel p can be simply calculated by averaging the pixel responses in RGB channels:

$$u_Y^P = (u_1^p + u_2^p + u_3^p)/3. \tag{2}$$

If we let $\bar{u}_n$ be the mean value of channel n, the pixel deviation δu_n^p, is

$$\delta u_m^p = u_n^p - \bar{u}_n, \tag{3}$$

and can be written in the vector form as

$$\delta \mathbf{u}^p = \mathbf{u}^p - \bar{\mathbf{u}}, \tag{4}$$

where $\delta \mathbf{u}^p = [\delta u_1^p, \delta u_2^p, \delta u_3^p]^T$, $\mathbf{u}^p = [u_1^p, u_2^p, u_3^p]^T$, and $\bar{\mathbf{u}} = [\bar{u}_1, \bar{u}_2, \bar{u}_3]^T$, with superscript T representing the vector transpose. Similarly, the pixel deviation δu_Y^P of channel Y can be computed as

$$\delta u_Y^P = u_Y^P - \bar{u}_Y, \tag{5}$$

where $\bar{u}_Y$ is the mean value of channel Y.

For color images, the pixel responses of RGB channels are not independent, but rather are highly correlative.[9] The channel correlation of color texture image is the basis of the statistical models for texture and color fusion, especially when only 1-D spatial distribution (for example, channel Y) is known *a priori*. The correlation coefficient c_n between channel n and Y can be calculated according to

$$c_n = \frac{\sum_p \delta u_n^p \times \sum_p \delta u_Y^P}{\left[\sum_p (\delta u_n^p)^2 \times \sum_p (\delta u_Y^P)^2\right]^{1/2}}. \tag{6}$$

A typical color texture image and its pixel deviation distributions of RGB channels with respect to Y channel are given in Fig. 1. The angles of the mean axis of the point clouds define the degrees of correlation, with 0 and 90 deg indicating uncorrelated data. The correlation coefficient of the blue channel, 0.988, is the highest, followed by that of the red channel, 0.985. The correlation coefficient of the green channel, 0.915, is the lowest. These observations clearly indicate the existence of high channel correlation of texture images.

It is of interest to investigate the hue distribution of single-colored texture images. For pixel p, the hue can be calculated as[12]

$$H^p = \arctan\left[\frac{\sqrt{3}(u_2^p - u_1^p)}{2u_3^p - u_1^p - u_2^p}\right]. \tag{7}$$

Figure 2 shows a histogram of the texture image in Fig. 1. It is found that despite the heavy textures, the hue is con-

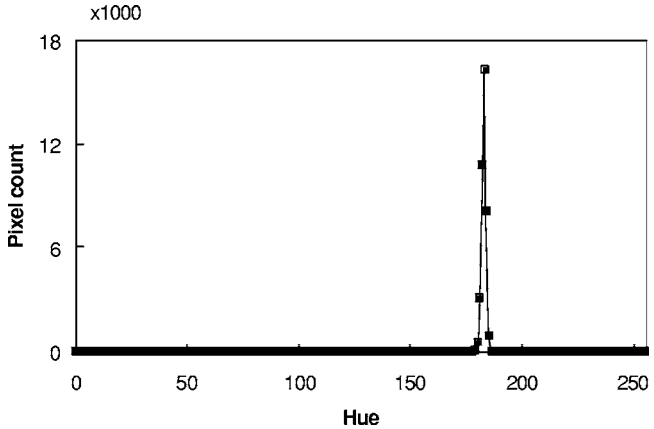

Fig. 2 Histogram of hue of the texture image in Fig. 1. The hue is scaled to the range of 0 to 255.

strained in a very limited range and thus can be considered to be approximately constant. This also explains why hue is always used in color image segmentation.[12]

In addition to the statistical analysis of texture images, it is also interesting to discuss the physical interaction between object surface and lighting. According to the dichromatic reflection model,[8] the reflected light can be decomposed into two components, i.e., surface reflection and body reflection. The surface reflection occurs at the object surface, and its spectral composition is approximately the same as that of the illumination. The body reflection is the result of the scattering of the light within the pigmented layer of the object subsurface, and the selective absorption of the light dependent on the material characteristic. According to the neutral interface reflection (NIR) model,[13] the reflectance $r(\lambda,p)$ is represented as

$$r(\lambda,p) = m_b^p r_b(\lambda) + m_s^p r_s, \tag{8}$$

where m_b^p and m_s^p are the geometric factors of the body and surface reflections at pixel p, $r_b(\lambda)$ is the wavelength composition of the body reflectance, and r_s is the constant surface reflectance independent of wavelength. Substituting Eq. (8) into Eq. (1) yields

$$\begin{aligned} u_n^p &= m_b^p \int l(\lambda) r_b(\lambda) s_n(\lambda)\, d\lambda + m_s^p \int l(\lambda) s_n(\lambda) r_s\, d\lambda \\ &= m_b^p u_{b,n} + m_s^p I_n, \end{aligned} \tag{9}$$

where $u_{b,n}$ and I_n are the channel responses of body and surface reflections, respectively. Equation (9) can be written in the vector form as

$$\mathbf{u}^p = m_b^p \mathbf{u}_b + m_s^p \mathbf{I} \tag{10}$$

where $\mathbf{u}_b$ is the column vector of element $u_{b,n}$, and $\mathbf{I}$ is the column vector of element I_n. As the coefficient m_d^p and m_s^p describe the geometry of pixel p, Eq. (10) can be used to colorize textured samples or 3-D objects in a single image.[9,14]

The dichromatic reflection model can be applied to a variety of materials including plastic, wood, ceramic, and also the textile fabrics used in this study. However, the dichromatic reflection model may fail to describe other materials with nonneutral surface reflections such as coated glasses, iridescent surfaces, and some other textile fabrics including silk and satin.

3 Models for Fusion of Texture and Color

In this section, several computational models for fusion of texture and color are discussed. For simplicity and clarity, existing methods for texture and color fusion are classified into three models: gray-to-color mapping (GCM) model, color-to-color mapping (CCM) model, and dichromatic-based (DICH) model. As the CCM model can be applied in different color spaces, three methods, namely, CCM-RGB, CCM-$l\alpha\beta$, and CCM-LCH, are further discussed. For the DICH model, two methods, namely, DICH-GC and DICH-CC, are introduced for gray-scale and color original images, respectively.

3.1 *GCM Model*

The GCM model deals with the mapping of color to gray-scale images to produce desired color images. The essence of this model is to derive the 3-D spatial information (RGB) from the only known 1-D information (Y channel). This derivation is possible because of the high channel correlation of texture images discussed above. If the desired target color is $\bar{\mathbf{v}}$, and the standard deviations of channels n and Y are σ_n and σ_Y, respectively, then the color $\mathbf{v}^{\mathrm{GCM},p}$ of the reproduced image at pixel p can be calculated as[4]

$$\mathbf{v}^{\mathrm{GCM},p} = \bar{\mathbf{v}} + \mathbf{D}\,\delta\mathbf{u}_Y^P \tag{11}$$

where $\delta\mathbf{u}_Y^P = [\delta u_Y^P, \delta u_Y^P, \delta u_Y^P]^T$, and $\mathbf{D}$ is a 3×3 diagonal matrix diag $[\sigma_1^1, \sigma_2^1, \sigma_3^1]$, with $\sigma_n^1 = \sigma_n/\sigma_Y$. In the virtual coloring method, parameters are adopted to modify the standard deviation σ_n of each channel to obtain pleasing visual effects.[6] Since the purpose of this paper is to investigate the color fidelity of the model, the parameter of the virtual coloring method is not considered. When σ_n is unknown *a priori*, it can be assumed that $\sigma_n = \sigma_Y$, and $\mathbf{D}$ becomes an identity matrix diag [1,1,1]. In this case, the appearance of the simulated image is usually smoother than that of the actual target one.

According to Eq. (7), the hue of pixel p for the simulated image using GCM model becomes

$$\begin{aligned} H^p &= \arctan\left[\frac{\sqrt{3}\left(\bar{\nu}_2 + \sigma_2^1 \delta u_Y^P - \bar{\nu}_1 - \sigma_1^1 \delta u_Y^P\right)}{2\left(\bar{\nu}_3 + \sigma_3^1 \delta u_Y^P\right) - \left(\bar{\nu}_1 + \sigma_1^1 \delta u_Y^P\right) - \left(\bar{\nu}_2 + \sigma_2^1 \delta u_Y^P\right)}\right] \\ &= \arctan\left\{\frac{\sqrt{3}\left[\left(\bar{\nu}_2 - \bar{\nu}_1\right) + \left(\sigma_2^1 - \sigma_1^1\right)\delta u_Y^P\right]}{\left(2\bar{\nu}_3 - \bar{\nu}_1 - \bar{\nu}_2\right) + \left(2\sigma_3^1 - \sigma_1^1 - \sigma_2^1\right)\delta u_Y^P}\right\}. \end{aligned} \tag{12}$$

It is obvious that when $\sigma_1 \approx \sigma_2 \approx \sigma_3$, the hue of each pixel p is a constant absolutely decided by the target color $\bar{\mathbf{v}}$. For real texture images, when σ_n does not differ much with each other, the variation of hue is very small, which is in agreement with the observation in Sec. 2.

3.2 *CCM Model*

Unlike the GCM model, the original image of the CCM model is colored, and thus it is a 3-D-to-3-D color-mapping problem. In the RGB color space, if the pixel deviation is unchanged in color mapping, the new color at pixel p can be simply calculated by subtracting mean color $\bar{\mathbf{u}}$ and adding target color $\bar{\mathbf{v}}$ as follows:

$$\mathbf{v}^{\mathrm{CCM\text{-}RGB},p} = \bar{\mathbf{v}} + \mathbf{u}^p - \bar{\mathbf{u}} = \bar{\mathbf{v}} + \delta\mathbf{u}^p. \tag{13}$$

However, as the investigation of texture image found that the pixel deviation is actually related to the mean color, it is more appropriate to calculate $\mathbf{v}^{\mathrm{CCM\text{-}RGB},p}$ as[5]

$$\mathbf{v}^{\mathrm{CCM\text{-}RGB},p} = \bar{\mathbf{v}} + f(\bar{\mathbf{v}} + \delta\mathbf{u}^p), \tag{14}$$

where function $f(\cdot)$ is defined on each pixel position and performs linear interpolation between (u_1^p, u_2^p, u_3^p) and $(\delta u_1^p, \delta u_2^p, \delta u_3^p)$. The plot of function $f(\cdot)$ is shown in Fig. 3, in which $u_1^p < u_2^p < u_3^p$ is assumed. To not introduce extrapolation error, the value of function $f(\cdot)$ is clipped to δu_1^p and δu_3^p in the ranges of $[0, u_1^p]$ and $[u_3^p, 255]$, respectively.

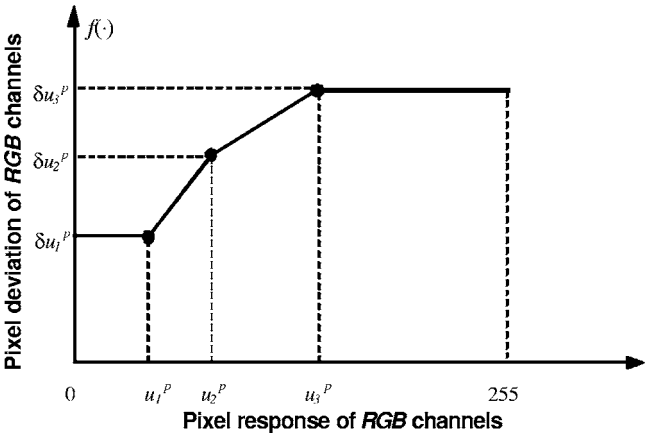

Fig. 3 Function $f(\cdot)$ for the CCM model in RGB color space.

In addition to the RGB space, the CCM model can also be applied[10,11] in other color spaces such as $l\alpha\beta$ and CIELCH. The $l\alpha\beta$ space was first proposed by Ruderman *et al.* based on the principle component analysis (PCA) of many natural scene images.[15] In the transform, the RGB space is first linearly transformed to LMS space, then to a logarithmic space, and finally is rotated to produce $l\alpha\beta$ color space. The detailed transformation can be found in Refs. 10 and 15. An advantage of the $l\alpha\beta$ space is that the channel correlation was eliminated, and therefore the modification of the response in one channel would minimally affect those in other channels. In the $l\alpha\beta$ space, the new $l\alpha\beta$ color $\mathbf{v}^{\text{CCM-}l\alpha\beta,p}$ of pixel p can be written as[10]

$$\mathbf{v}^{\text{CCM-}l\alpha\beta,p} = [\bar{l}', \bar{\alpha}', \bar{\beta}']^T + [l^p, \alpha^p, \beta^p]^T - [\bar{l}, \bar{\alpha}, \bar{\beta}]^T, \tag{15}$$

where $[\bar{l}, \bar{\alpha}, \bar{\beta}]^T$ is the mean color of the original image, $[l^p, \alpha^p, \beta^p]^T$ is the color of pixel p in the image, and $[\bar{l}', \bar{\alpha}', \bar{\beta}']^T$ is the desired target color. Note that the standard deviation of each channel is not considered in Eq. (15). The last step of the CCM-$l\alpha\beta$ method is to transform the new $l\alpha\beta$ color back to RGB space.

In the study of the texture effect on suprathreshold lightness tolerances, Montag and Berns presented a method of texture image simulation in CIELCH color space.[11] They first rotate the CIELCH color space using a 3×3 matrix based on PCA to produce a decorrelated space, and then modified the mean color of the image, and finally inverted the color transform to generate new texture images. When the purpose is to simulate a new image using the same texture and different color, the PCA is no longer required.[11] Therefore, similar to Eq. (15), the new color $\mathbf{v}^{\text{CCM-LCH},p}$ of pixel p in CIELCH space can be calculated as follows:

$$\mathbf{v}^{\text{CCM-LCH},p} = [\bar{L}', \bar{C}', \bar{h}']^T + [L^p, C^p, h^p]^T - [\bar{L}, \bar{C}, \bar{h}]^T, \tag{16}$$

where $[\bar{L}, \bar{C}, \bar{h}]^T$ is the mean color of the original image, $[L^p, C^p, h^p]^T$ is the color of pixel p in the original image, and $[\bar{L}', \bar{C}', \bar{h}']^T$ is the desired target color in CIELCH space. Similar to the CCM-$l\alpha\beta$ method, $\mathbf{v}^{\text{CCM-LCH},p}$ should also be converted back to RGB space.

3.3 *DICH Model*

The GCM and CCM models are both based on the statistical distribution of texture images. Considering the spatial color distribution of texture images is attributed to the geometrical structures of the texture samples, Shen and Xin proposed a texture rendering method based on the dichromatic reflection model.[9] According to Eq. (10), the channel responses $\mathbf{u}^p$ can be decomposed into two body color $\mathbf{u}_b$ and surface color $\mathbf{I}$. If N denotes the pixel number of a texture image, the mean color $\bar{\mathbf{u}}$ can be written as

$$\bar{\mathbf{u}} = \frac{1}{N}\sum_p \mathbf{u}^p = \frac{1}{N}\left(\sum_p m_b^p\right)\mathbf{u}_b + \frac{1}{N}\left(\sum_p m_s^p\right)\mathbf{I} = \bar{m}_b\mathbf{u}_b + \bar{m}_s\mathbf{I}, \tag{17}$$

where $\bar{m}_b$ and $\bar{m}_s$ are the mean geometric coefficients of the body and surface colors, respectively. The surface color $\mathbf{I}$ is actually the white point of the imaging system, and can be obtained by imaging an ideal white diffuser. For images where we lack knowledge of the imaging condition, for example, those downloaded from the Internet, we suppose the camera is white balanced to the light source and thus $\mathbf{I}=[255,255,255]^T$.

We can combine Eqs. (10) and (17) by eliminating term $\mathbf{u}_b$ as

$$\mathbf{u}^p = a^p\bar{\mathbf{u}} + b^p\mathbf{I}, \tag{18}$$

where

$$a^p = \frac{m_b^p}{\bar{m}_b}, \quad b^p = \frac{m_s^p\bar{m}_b - m_b^p\bar{m}_s}{\bar{m}_b}. \tag{19}$$

From Eq. (18), the relationship between $\mathbf{u}^p$ and $\bar{\mathbf{u}}$ is completely specified by the geometric coefficient pair (a^p, b^p).

In the case where the original texture image is of a color other than the white point $\mathbf{I}$, the geometric coefficients pair (a^p, b^p) in Eq. (18) can be solved by the least-squares method. The new color $\mathbf{v}^{\text{DICH-CC},p}$ can then be calculated as

$$\mathbf{v}^{\text{DICH-CC},p} = a^p\bar{\mathbf{v}} + b^p\mathbf{I}. \tag{20}$$

In the case where the original image is a gray-scale image, that is, only 1-D information of the Y channel is available, the coefficients could be solved by neglecting surface reflection as

$$a^p = \frac{u_Y^P}{\bar{u}_Y}, \quad b^p = 0, \tag{21}$$

and the calculation of new color can be simplified as

$$\mathbf{v}^{\text{DICH-GC},p} = \frac{u_Y^P}{\bar{u}_Y}\bar{\mathbf{v}}. \tag{22}$$

From Eqs. (20) and (22), it is obvious that $\mathbf{v}^{\text{DICH-GC},p}$ is a special case of $\mathbf{v}^{\text{DICH-CC},p}$. Note that Eq. (22) will produce larger errors than Eq. (20) in simulating a texture image with unneglectable surface reflections.

Without loss of generality, the image can be normalized with respect to the white point $\mathbf{I}$. Then, for the DICH model, the hue of pixel p can be calculated as

Fig. 4 Examples of the texture images used in the study. The images of the two rows are of the same texture patterns and different colors.

$$H^p = \arctan\left[\frac{\sqrt{3}(a^p\bar{\nu}_2 + b^p 255 - a^p\bar{\nu}_1 - b^p 255)}{2(a^p\bar{\nu}_3 + b^p 255) - (a^p\bar{\nu}_1 + b^p 255) - (a^p\bar{\nu}_2 + b^p 255)}\right] = \arctan\left[\frac{\sqrt{3}(\bar{\nu}_2 - \bar{\nu}_1)}{2\bar{\nu}_3 - \bar{\nu}_1 - \bar{\nu}_2}\right]. \quad (23)$$

It is found that the hue is a constant for every pixel p, which is the same as in the GCM model when $\sigma_n = \sigma_Y$ [see Eq. (12)].

4 Experiments and Discussion

To study the color fidelity of the three computational models for texture and color fusion, textile fabrics with different texture patterns were used. The texture images were obtained by scanning these fabrics using an Epson scanner model GT10000+ at a resolution of 72 dpi. Some examples of the texture images are shown in Fig. 4.

We further define texture strength as the standard deviation of the texture image in this study. It is known that texture strength is related to the mean colors of the texture images.[9] For example, for certain materials, the texture strength may be small in the dark intensity range, while it is large in the light intensity range. Therefore, it is worthwhile to investigate the color fidelity of these methods in two cases. The first case assumes that the standard deviation of the target image is unknown *a priori*, and thus no adjustment of the texture strength is applied. The second case assumes that the standard deviation of the target image is known, and thus the texture strength of the simulated image can be adjusted as follows.

If the standard deviations of the n'th channel of the reproduced and target images are σ_n^N and σ_n^T, respectively, the final new color $\nu_n^{p,T}$ after texture strength adjustment can be calculated in the RGB color space as

$$\nu_n^{p,T} = \bar{\nu}_n + \frac{\sigma_n^T}{\sigma_n^N}\left(\nu_n^p - \bar{\nu}_n\right). \quad (24)$$

The performances of the models can be evaluated by comparing the simulated texture image with the target image. As there is no pixel correspondence for the simulated and target texture images, the evaluation is conducted using a statistical approach.

The similarity of the simulated and the target images must be evaluated in perceptually uniform color spaces such as CIELAB and CIELUV. In the textile and apparel industry, the CIELAB space is generally used. In the experiment, texture images were displayed on a calibrated and characterized SONY Tinitron 21-in. CRT display. The characterization of the display was carried out using the gain, offset, and gamma (GOG) model,[16] and the RGB values of the texture images can be transformed to the corresponding CIELAB values according to the model. For each pixel, its color difference ΔE_{ab}^* to the mean color is calculated in the CIELAB space. The histogram of the color difference was then constructed, in which each bin denotes an interval of 0.5 unit of ΔE_{ab}^*.

Assume that B_T is the target texture image, B_S is the simulated image, and $H_j(\cdot)$ is the pixel count of the j'th bin of the histogram, then the image similarity ratio $s(B_S, B_T)$ between these two images can be calculated by histogram intersection[17] as

$$s(B_T, B_S) = \frac{\sum_{j=1}^{M} \min\left[H_j(B_T), H_j(B_S)\right]}{\sum_{j=1}^{M} H_j(B_T)}, \quad (25)$$

where M is the number of bins of the histogram. When the texture distributions of the two images B_T and B_S are quite similar, the term $s(B_S, B_T)$ should be appropriate for the assessment of the image similarity in terms of color fidelity. The more similar the target image is to the simulated image, the closer is the image similarity ratio $s(B_S, B_T)$ is to 1.

Figure 5 gives the simulation results for the computational models for texture and color fusion without texture strength adjustment. The original and target images are of the same texture pattern, and the mean color of the target image is used as target color. It is found that all of the fusion results are perceptually very close to the target.

In the experiment, 40 different texture images were randomly selected to compare the color fidelity of the computational models in terms of image similarity according to Eq. (25). The mean image similarity ratio and the standard

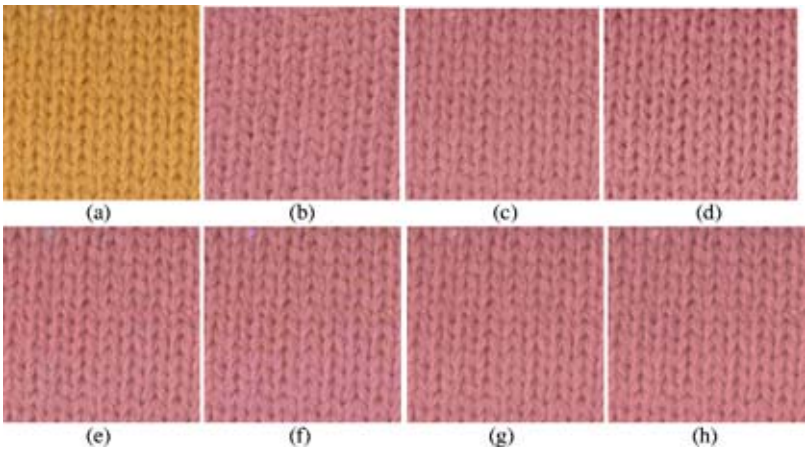

Fig. 5 Simulated results using different methods: (a) original, (b) target, (c) GCM, (d) CCM-RGB, (e) CCM-LCH, (f) CCM-$l\alpha\beta$, (g) DICH-CC, and (h) DICH-GC.

deviation between target and simulated images are shown in Fig. 6. It is found that, when no texture strength adjustment is applied, the DICH-CC method performs the best, followed by the CCM-RGB and CCM-LCH methods. The similarity ratios of the GCM and DICH-GC methods are very close, but both are lower than those of the DICH-CC, CCM-RGB, and CCM-LCH methods. It is surprising that the CCM-$l\alpha\beta$ method performs the worst. It was also found in the experiments that the CCM-$l\alpha\beta$ method sometimes produces false colors in shadow areas of texture images. The reason may be that the $l\alpha\beta$ space is derived from natural scene images other than textile texture images used in this study.[15] In the case of texture strength adjustment, the

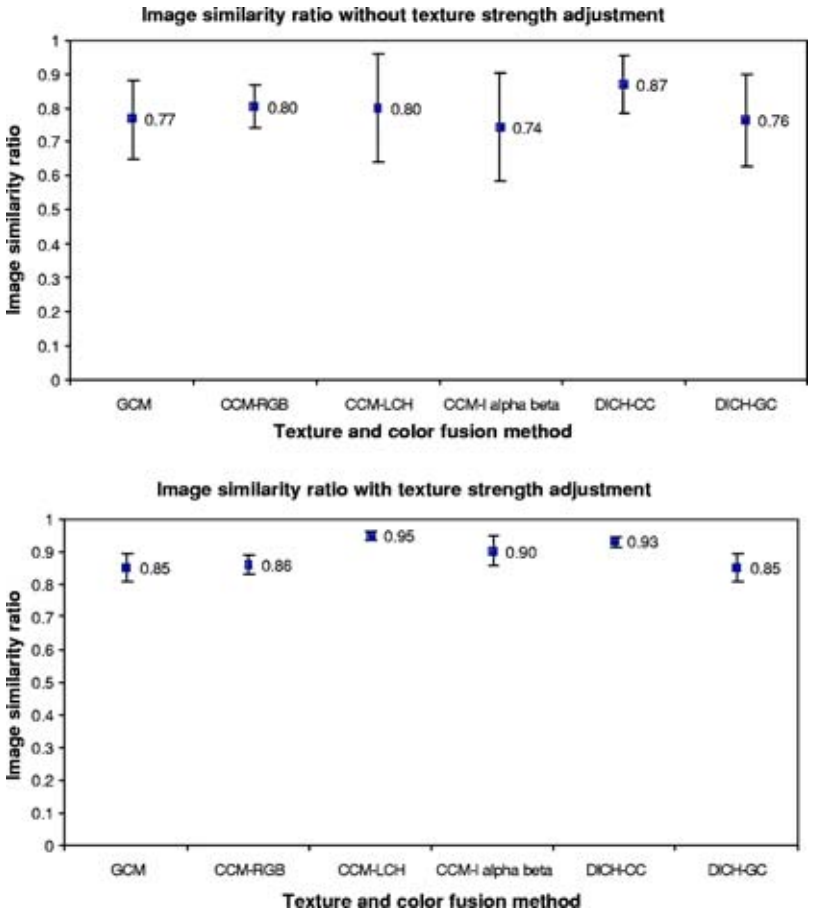

Fig. 6 Image similarity ratio (±1 standard deviation) between simulated and target images for different texture and color fusion methods, without (top) and with (bottom) texture strength adjustment.

color fidelity of each method is greatly improved. The image similarity of the CCM-LCH method is the highest at 0.95, followed by the DICH-CC method, which is 0.93. The third is the CCM-$l\alpha\beta$ method, at about 0.90. The similarity ratios of the GCM, CCM-RGB, and DICH-GC methods are all about 0.85.

From the two plots in Fig. 6, the variation of similarity ratios is much smaller after applying texture strength adjustment. By holistic consideration of these two cases, it can be concluded that the CCM-LCH and DICH-CC methods are more appropriate for texture and color fusion when the original image is color, while either the GCM or the DICH-GC method can be used for texture and color fusion when the original image is of gray scale.

5 Conclusion

We studied the performance of different computational models for texture and color fusion in terms of color fidelity. As the texture strength is related to the mean color of the image, two cases—with or without texture strength adjustment—were introduced. The color fidelity of these texture and color fusion methods was studied in terms of image similarity between the simulated and target images. When the texture strength is not applied, the DICH-CC method is the best, followed by the CCM-RGB and CCM-LCH methods. When the texture strength is applied, the image similarity ratio for each method is significantly improved. The color accuracy of the CCM-LCH method is the highest, followed by the DICH-CC and CCM-$l\alpha\beta$ methods. The performance of the GCM and DICH-GC methods are acceptable considering there is only 1-D spatial information available in the original gray-scale image.

The physical samples used in this study are limited to the certain textile fabrics. In future research, it is of our interest to evaluate these different computational models on other textile materials including pile and wool fabrics. In addition, some texture recognition and classification methods in the image processing literature will also be considered for the evaluation of these texture and color fusion models.

Acknowledgments

The authors would like to acknowledge the financial support of this project from the Hong Kong Polytechnic University and the Research Grants Council of Hong Kong SAR Government (project reference: PolyU 5153/01E).

References

1. E. Ozyildiz, N. Krahnstover, and R. Sharma, "Adaptive texture and color segmentation for tracking moving objects," *Pattern Recogn.* **35**, 2013–2029 (2002).
2. P. Campisi and G. Scarano, "A multiresolution approach for texture synthesis using the circular harmonic functions," *IEEE Trans. Image Process.* **11**, 37–51 (2002).
3. J. C. Russ, *The Image Processing Handbook*, 4th ed., CRC Press, New York (2002).
4. J. H. Xin and H. L. Shen, "Computational model for color mapping on texture image," *J. Electron. Imaging*, **12**, 697-704 (2003).
5. J. H. Xin and H. L. Shen, "Recolouring digital textile printing design with high fidelity," *Color. Technol.* **120**, 6–13 (2004).
6. V. Botchko, S. Nakauchi, J. Parkkinen, and H. Kalviainen, "Multispectral texture derivation in virtual coloring," in *Texture Analysis in Machine Vision*, M. K. Pietikainen, Ed., pp. 113–126, World Scientific, London (2000).
7. V. Botchko, T. Jaaskelainen, and J. Parkkinen, "Multispectral texture model for color and highlight reproduction," in *Proc. IS&T 1st Eur. Conf. on Colour in Graphics, Image, and Vision*, pp. 603–607 (2002).
8. S. A. Shafer, "Using color to separate reflection components," *Color Res. Appl.* **10**, 210–218 (1985).
9. H. L. Shen and J. H. Xin, "Dichromatic based rendering of texture images with high color fidelity," *J. Imaging Sci. Technol.* **48**, 233–237 (2004).
10. E. Reinhard, M. Ashikhmin, B. Gooch, and P. Shirley, "Color transfer between images," *IEEE Comput. Graphics Appl.* **21**, 34–41 (2001).
11. E. D. Montag and R. S. Berns, "Lightness dependencies and the effect of texture on suprashreshold lightness tolerances," *Color Res. Appl.* **25**, 241–249 (2000).
12. T. Gevers and A. W. M. Smeulders, "PicToSeek: combining color and shape invariant features for image retrieval," *IEEE Trans. Image Process.* **9**, 102–119 (2000).
13. H. C. Lee, E. J. Breneman, and C. P. Schulte, "Modeling light reflection for computer color vision," *IEEE Trans. Pattern Anal. Mach. Intell.* **12**, 402–409 (1990).
14. J. H. Xin and H. L. Shen, "Accurate color synthesis of three-dimensional objects in an image," *J. Opt. Soc. Am. A* **21**, 713–723 (2004).
15. D. L. Ruderman, T. W. Cronin, and C. C. Chiao, "Statistics of cone response to natural images: implications for visual coding," *J. Opt. Soc. Am. A* **15**, 2036–2045 (1998).
16. R. S. Berns, R. J. Motta, and M. E. Gorzynski, "CRT colorimetry. Part I: theory and practice," *Color Res. Appl.* **18**, 299–314 (1993).
17. M. J. Swain and D. H. Ballard, "Color indexing," *Int. J. Comput. Vis.* **7**, 11–32 (1991).

Hui-Liang Shen received his BE and PhD degrees in information science and electronic engineering from Zhejiang University, China, in 1996 and 2002, respectively. He is currently a research associate with the Institute of Textiles and Clothing, the Hong Kong Polytechnic University. His research interests are color imaging, computer vision, and image processing.

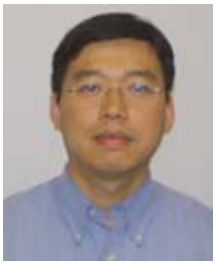

John H. Xin graduated with a PhD degree from the University of Leeds, United Kingdom, in 1989 and became a technologist in the color section of the Research and Development Department of the multinational textile company Coats Viyella, United Kingdom. He became a project coordinator for the development of a new-generation computer color management and color quality control system with the University of Derby, United Kingdom, in 1994. In 1996 he joined the Institute of Textiles and Clothing, the Hong Kong Polytechnic University, where he is currently an associate professor. His research interests are color management, digital color communication and reproduction, and the psychological aspects of color. He is a charted colourist, awarded by the Society of Dyers and Colorists, United Kingdom.